Journal of Materials Processing Technology 211 (2011) 1184–1190

Contents lists available at ScienceDirect

Journal of Materials Processing Technology

journal homepage: www.elsevier.com/locate/jmatprotec

Effects of ARB and ageing processes on mechanical properties and microstructure of 6061 aluminum alloy

Mohammad Reza Rezaei*, Mohammad Reza Toroghinejad, Fakhreddin Ashrafizadeh

Department of Materials Engineering, Isfahan University of Technology, Isfahan 84156-83111, Iran

ARTICLE INFO

Article history:
Received 19 August 2010
Received in revised form 18 January 2011
Accepted 28 January 2011
Available online 4 February 2011

Keywords:
Aluminum alloys
Accumulative roll bonding
Ageing treatment
Mechanical properties

ABSTRACT

Accumulative roll bonding (ARB) has been used as a severe plastic deformation process for the production of high-strength materials. Ageing treatment has been found to enhance the strength of alloys by precipitation of a second phase. In the present work, ARB followed by the ageing process was used for the fabrication of the high-strength 6061 aluminum alloy. Samples of the alloy thus made were subjected under annealed and ARBed conditions to ageing treatment at different temperatures for different times and their mechanical properties were evaluated. It was found that the microhardness and tensile strength of the specimens increased with the number of ARB cycles but their elongation values decreased. After the ageing treatment, the mechanical properties of the ARBed specimens improved in terms of both strength and ductility. Based on TEM observations, it may be concluded that the improved mechanical properties after the duplex ARB-ageing process can be attributed to the precipitation of very fine particles with a slight decrease in dislocation density and limited structure coarsening. SEM observation of fracture surfaces of aged specimens indicated that the fracture was predominantly caused by microvoid coalescence at constituent particles.

1. Introduction

The low density of aluminum alloys combined with their high strength has made them the material of primary choice for aircraft applications where specific strength (strength-to-weight ratio) is a major design consideration as pointed out by Liu et al. (2003). Aluminum–magnesium–silicon (Al–Mg–Si) denoted by 6XXX series alloys are medium-strength, heat-treatable alloys known for their excellent formability and good corrosion resistance. Mg and Si are the major solutes; they increase the strength of the alloy by precipitation hardening. AA6061 is one of the most widely used alloys in this series that can be heat treated to produce precipitation to various degrees. The T6 treatment, involving solution heat treatment and quenching with subsequent artificial ageing, is a common method to increase the strength of this alloy as described by Abis et al. (1985). According to Kim and Wang (2007), the age hardening peaks of Al–Si–Mg alloys are correlated to their precipitation sequence: namely, decomposition of supersaturated solid solution, formation and dissolution of GP zones, transition phase and precipitated equilibrium phase: SSSS → GP zones → β″ → β′ → β (Mg_2Si) phase. The structure of β″, β′ and β phases is monoclinic (or hexagonal), hexagonal and cubic respectively, as pointed out by Davis (2000). Gleiter (2000) has shown that ultra-fine grained (UFG) and nanocrystalline materials are often harder, stronger, and more wear-resistant than their coarse grained counterparts. Recent developments in the fabrication of UFG materials have focused on the use of large strain or severe plastic deformation (SPD) as a method of producing high-strength metals and alloys. Experiments conducted by Apps et al. (2003) indicate that, besides strain hardening, there are other strengthening mechanisms used for metallic materials; precipitation strengthening is one such mechanism commonly employed for strengthening many commercial aluminum alloys.

Several novel SPD techniques have been developed for high-strength metals with minimal changes in the initial sample dimensions. These include equal channel angular pressing (ECAP), high pressure torsion (HPT), multi-axial forging (MAF), constrained groove pressing (CGP), and accumulative roll bonding (ARB). Among these processes, the accumulative roll-bonding process developed by Saito et al. (1999) has several advantages over other SPD processes: (1) no need for forming facilities with large load capacity and expensive dies; (2) high productivity; and (3) unlimited production. Due to its capability as a continuous process, only ARB is appropriate for manufacturing nanocrystalline and ultrafine grained sheets and plates which are the most widely used forms of commercial products.

Park et al. (2001) and Lee et al. (2002) applied the ARB process to 6061 aluminum alloys and investigated the microstructure and mechanical properties of ARBed samples. However, no conclusive research has been reported on the mechanical properties of

* Corresponding author. Tel.: +98 912 5321577.
E-mail address: mr.rezaei@ma.iut.ac.ir (M.R. Rezaei).

0924-0136/$ – see front matter © 2011 Elsevier B.V. All rights reserved.
doi:10.1016/j.jmatprotec.2011.01.023

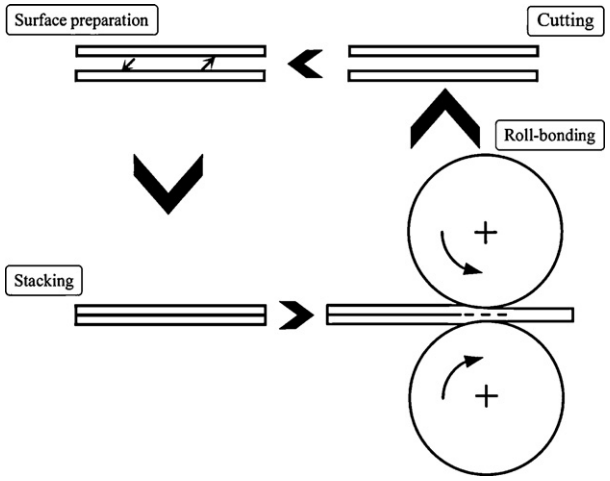

Fig. 1. Schematic illustration of the ARB process.

this alloy treated by post-ARB ageing. In the present study, the ARB process (with different numbers of cycles) and ageing treatment (at different temperatures and for times) were applied to a 6061 aluminum alloy. The mechanical properties of the samples, including their microhardness, tensile strength, and elongation, were studied. The results were correlated to TEM observations and SEM fracture modes.

2. Experimental procedure

As-received 6061 aluminum alloy was cut into 200 mm × 40 mm × 1 mm pieces parallel to the sheet rolling direction. The alloy had been annealed at 803 K for 1.5 h in an electrical furnace (specifications are given in Table 1) and then quenched into water prior to cutting.

To produce a satisfactory bond in ARB, it is essential to remove contaminants from the surfaces of the two metals to be bonded. These include oxides, adsorbed (sulfur, phosphor, and oxygen) ions, and grease, humidity, and dust particles. Tylecote (1968) and Bay (1986) have stated that the best method for surface preparation is degreasing followed by scratch brushing with a rotating steel brush. Therefore, the preparation processes for the specimens included degreasing in an acetone bath followed by scratch-brushing with a stainless steel brush wire 0.26 mm in diameter. It is important not to touch the cleaned surfaces, because grease or oil on the faying surfaces impairs the formation of a strong joint. To avoid any oxide formation or interference with bonding, the roll-bonding process must be carried out immediately after degreasing and scratch brushing.

The ARB process was carried out with no lubrication, using a laboratory rolling mill with a loading capacity of 20 tons. The roll diameter was 125 mm, and the rolling speed was set at 2 m/min. The roll-bonding process was carried out with a specific reduction equal to 50%. The roll-bonded strips were cut in half. The same procedure was repeated up to five cycles at ambient temperature. The ARB process is schematically illustrated in Fig. 1.

In order to investigate the effects of ageing treatments, the following three procedures were applied to the annealed samples (Fig. 2):

1. ageing treatment at 373 or 473 K;
2. accumulative roll bonding at room temperature; and
3. accumulative roll bonding at room temperature followed by ageing treatment at 373 or 473 K.

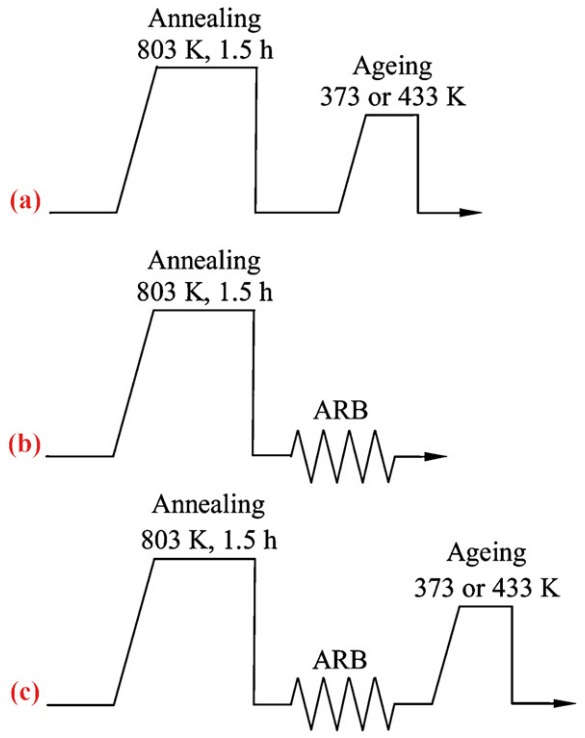

Fig. 2. Heat treatment process diagram for (a) as-aged sample, (b) ARBed sample, and (c) post-ARB aged sample.

The microstructure of the specimens was characterized on the RD-TD plane under a Philips CM12 transmission electron microscope (TEM) operating at 120 kV. Thin foil samples were prepared by twin-jet electropolishing in a A2 Struers solution containing 72 ml ethanol, 20 ml 2-butoxyethanol, and 8 ml perchloric acid (71% concentration) at −3 °C. The electropolish voltage was 35 V. In order to clarify the failure mode, fracture surfaces after tensile tests were observed by PHILIPS XL30 scanning electron microscopy (SEM). Vickers microhardness testing was performed using a LEITZ apparatus under a load of 100 g on the RD-TD plane of the samples. Microhardness was measured randomly at eight different points for each sample. Maximum and minimum values were disregarded, and the mean value was calculated using the remaining six values. The tensile test specimens were machined from the rolled sheets according to the ASTM E8M standard, oriented along the rolling direction (Fig. 3). The gauge length and the width of the tensile test specimens were 25 and 6 mm, respectively. Tensile tests were conducted at ambient temperature on a Houndsfield H50KS testing machine at a strain rate of $1.67 \times 10^{-4}\ s^{-1}$. Total elongation of the samples was measured as the difference between the gauge lengths before and after testing. The tensile test was repeated 3 times for each sample.

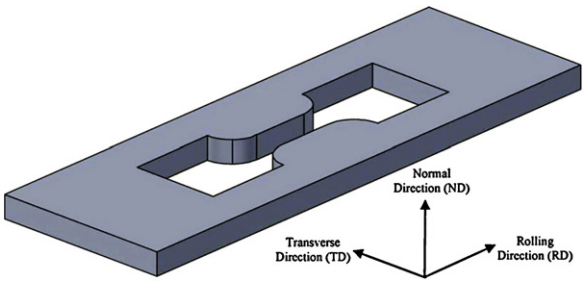

Fig. 3. Orientation of the tensile test specimens.

Table 1
Specifications of the 6061 aluminum alloy.

Material	Chemical composition (wt.%)	Condition	Tensile strength (MPa)	Elongation (%)	Microhardness ($HV_{0.1}$)
Al 6061	97.30Al, 1.16Mg, 0.63Si, 0.49Fe, 0.25Cu, 0.10Mn, 0.07 others	Annealed	162	19	47

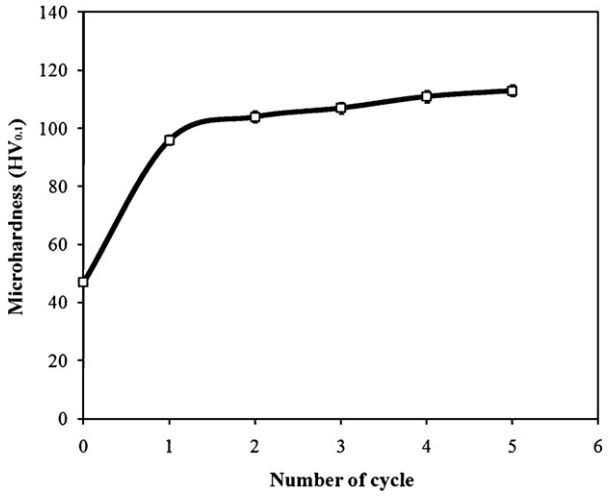

Fig. 4. Variations in microhardness versus number of ARB cycles.

3. Results and discussion

3.1. Microhardness

Fig. 4 shows the variations in microhardness values versus number of cycles. It can be seen that microhardness values increase with increasing number of cycles. Also, a sudden increase is observed in microhardness (~100%) after the first cycle (a strain level of 0.8), while only minor additional increases are detected afterwards up to the fifth cycle (a strain level of 4). The sudden increase at relatively low strains can be related to the formation of cell wall/subgrain boundaries rather than to grain refinement leading to strain hardening based on the density of dislocations and interactions between them as explained by Shaarbaf and Toroghinejad (2008).

Microhardness measurements after the ageing treatment at 433 K versus ageing time are shown in Fig. 5 for the annealed and ARBed specimens. As expected, the annealed (non-ARBed) specimen shows a remarkable increase (~100%) in microhardness with ageing time up to 18 h (where a peak value is observed). This can

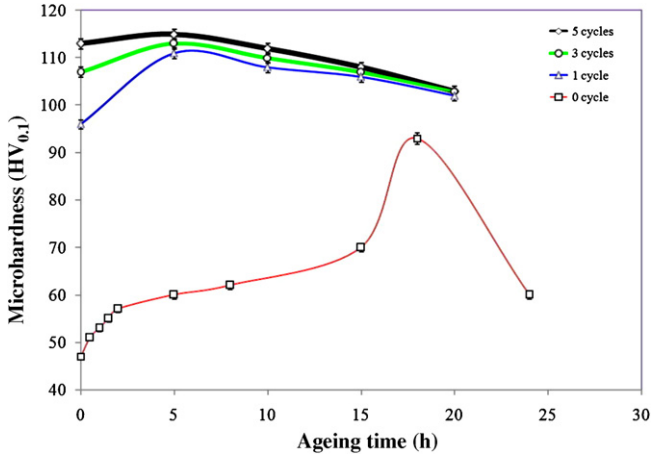

Fig. 5. Microhardness after the ageing treatment at 433 K versus ageing time for the annealed and ARBed specimens.

be attributed to the formation of metastable precipitates in the annealed specimen. After 18 h, microhardness decreases as a result of overageing. According to Edwards et al. (1998), the metastable β″ precipitate is considered to be responsible for the maximum age-hardening effect in this alloy. On the other hand, the formation of the β′ and β precipitates at the expense of losing coherence is largely associated with the reduction in hardness that occurs upon overageing. The ARBed specimen exhibits a different behavior from that of the annealed specimen in that its microhardness increases initially but declines after 5 h. These results can be explained by the interaction of four competing factors:

(1) dislocation-density reduction as a result of recovery;
(2) creation of non-shearable precipitates;
(3) depletion of solutes in the solid solution; and
(4) structure coarsening.

Microhardness decreases during ageing as recovery continues. Depletion of solutes in the solution during ageing will also decrease microhardness by removing the supersaturated solute atom atmosphere that drags dislocation motion. Creation of non-shearable precipitates during the ageing process, on the other hand, will cause microhardness to increase, and structure coarsening will reduce microhardness. Kim et al. (2001) have shown that, grain growth occurs in severely deformed metals at temperatures as low as 423–473 K.

The increasing microhardness at the beginning of the ageing treatment in the ARBed specimens may suggest that the creation of non-shearable precipitates outperforms the recovery of dislocations, the depletion of solutes in the solid solution, and the structure coarsening. However, further strengthening may not be readily realized since microhardness values begin to decline after 5 h at 433 K, which can be related to the dominance of dislocation-density reduction by recovery, depletion of the solutes in the solid solution, and structure coarsening over hardening effect by precipitation. Also precipitation coarsening and loss of precipitate coherence can be responsible for the decreased microhardness after ageing for 5 h at 433 K.

It is also clear from Fig. 5 that by increasing the number of cycles in the ARBed specimens, the slope of microhardness curve dwindles by up to 5 h of ageing. Additionally, the slop of the microhardness curve for the ARBed specimens decreases after 5 h of ageing at 433 K with increasing number of cycles. This can be explained by the stored deformation energy along the following lines. With increasing number of cycles, the stored deformation energy increases and the driving force for recovery and structure coarsening (two of the softening mechanisms), thereby, increases.

After the ageing treatment, the maximum values of microhardness in the annealed and ARBed (after 5 cycles) specimens were 93 and 115 $HV_{0.1}$, respectively. In other words, the ARBed specimen was harder than the annealed one at most by ~23%. Under this condition, the advantage of ARB processing does not seem to be very significant.

Fig. 6 shows the effect of ageing at 373 K on the microhardness of the annealed and ARBed specimens for different numbers of cycles. For the annealed (non-ARBed) specimen, microhardness increases slightly with ageing time and the peak ageing condition has not been reached even after 60 h. This can be again attributed to the formation of metastable precipitates in the annealed specimen. But, in this case, the ageing process performed at lower temperature

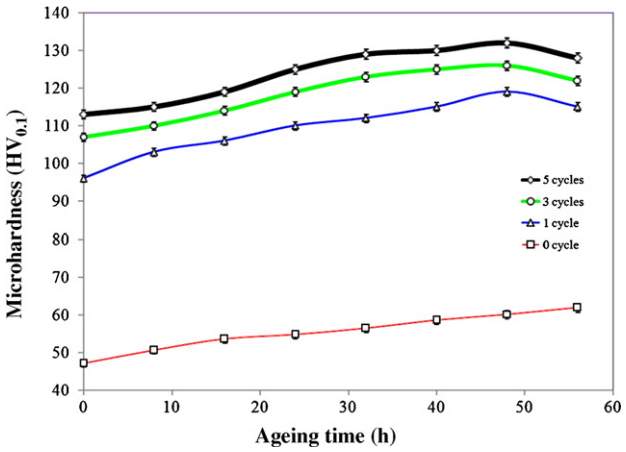

Fig. 6. Microhardness after ageing treatment at 373 K versus ageing time for annealed and ARBed specimens.

compared to ageing treatment at 433 K, causes diffusion to reduce and peak ageing condition has been reached in longer times (formation of precipitates is dependent on diffusion). In the case of the ARBed specimens, microhardness approaches its maximum value after 48 h, but it decreases with further ageing (after 56 h). These results are consistent with the findings of Kim et al. (2001), who showed in their investigation of the ECAPed 6061 aluminum alloy that the maximum value of hardness was obtained after 48 h of ageing at 373 K. With ageing at 373 K, a remarkable increase was observed in microhardness with ageing for all the ARBed specimens irrespective of the number of cycles. At this temperature, the softening effect of the ageing process is reduced.

Microhardness values for the annealed and 5-cycle ARBed specimens after ageing were 61 and 132 $HV_{0.1}$, respectively. In other words, the ARBed specimen was harder than the annealed one at most by ~114%. Thus, for ageing at 373 K, the advantage of ARB processing is noticeable. Comparison of Figs. 5 and 6 indicates that the maximum value of microhardness in the ARBed specimens was reached after a shorter ageing time. This shift is due to the accelerated precipitation as a result of the presence of higher density of dislocations.

3.2. Microstructure

Using the microhardness results during the ageing of the specimens, ageing treatments were carried out at 433 K for 5 h and 373 K for 48 h to investigate the microstructural features and tensile properties of the specimens. Fig. 7 shows the TEM micrographs for a 5-cycle ARBed specimen (Fig. 7(a)), a 5-cycle ARBed specimen after ageing at 433 K for 5 h (Fig. 7(b)), and a 5-cycle ARBed specimen after ageing at 373 K for 48 h (Fig. 7(c)). For the 5-cycle ARBed sample, nearly well defined ultra-fine grains surrounded by clear boundaries were formed. The mean size of the grains was about 240 nm. There are some dislocations within the interior of the grains. The ultra-fine grains slightly changed after ageing at 373 K for 48 h (grain size is about 280 nm) while dislocation density scarcely differed from that of the 5-cycle ARBed specimen. Dislocations are well retained after ageing, indicating low recovery during the ageing process. However, enormous nanosized particles appeared in the structure. Two kinds of particles can be observed in the TEM micrographs of all the specimens: some gray and some white. White and gray particles, which were analyzed by energy dispersive spectroscopy (EDS), are identified as Si-rich and Mg_2Si precipitates, respectively. The size of the Mg_2Si precipitates is larger than that of the Si-rich particles. In the sample aged at 373 K, most Mg_2Si precipitates have a globular or spherical shape with diame-

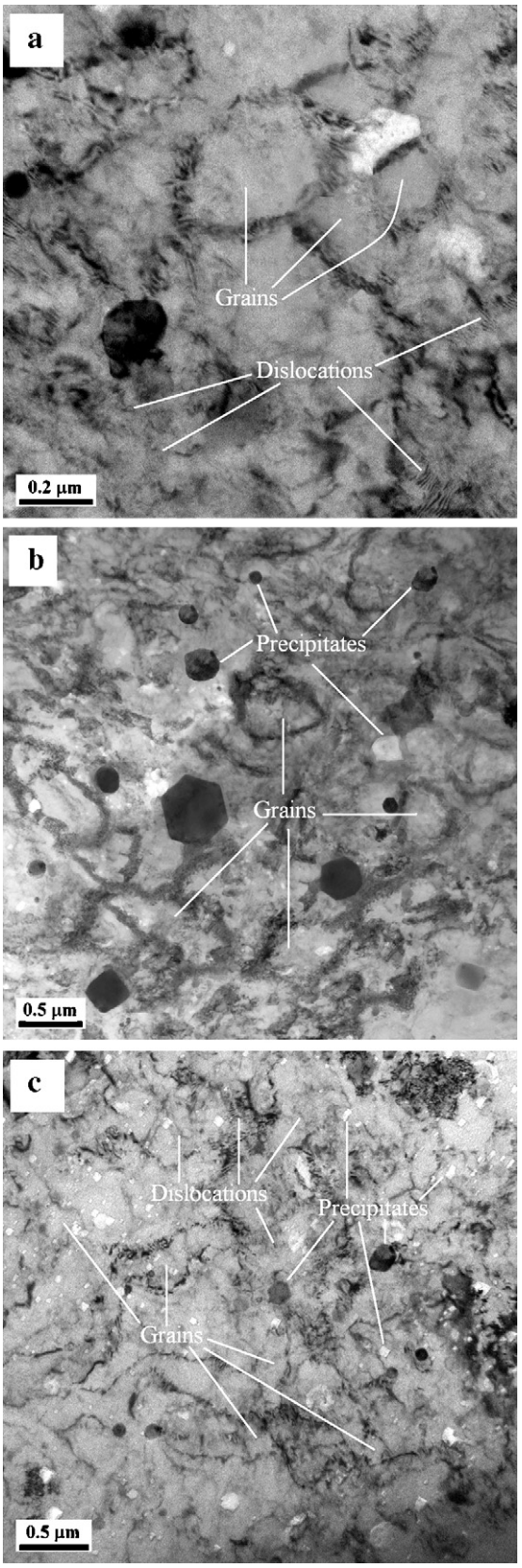

Fig. 7. Transmission electron micrographs of (a) 5-cycle ARBed and 5-cycle ARBed + aged specimens at (b) 433 K for 5 h and (c) 373 K for 48 h.

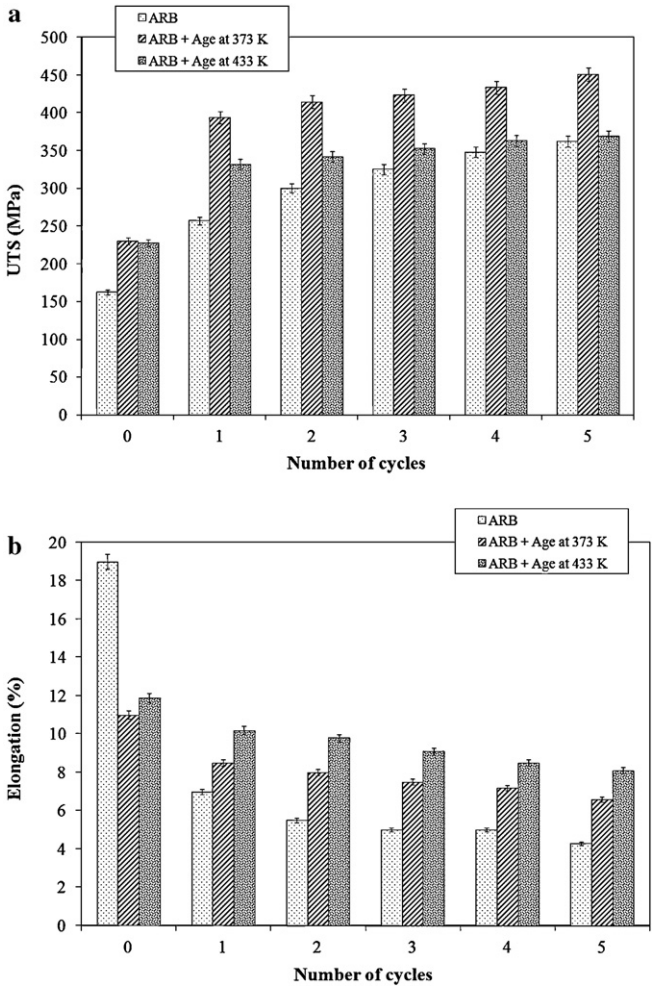

Fig. 8. Variations in (a) UTS and (b) elongation values versus number of cycles for different heat treatment conditions.

ters ranging from 40 to 90 nm. It can, therefore, be concluded that the outstanding hardening effect of the post-ARB ageing for this time and at this temperature is related to the presence of high dislocation density and fine precipitates. After ageing at 433 K for 5 h, softening features were identified. In this situation, some structure coarsening happened (grain size is about 380 nm) and the density of dislocations was reduced.

Note that the particle morphology (globular or spherical) observed in both ageing conditions is different from that commonly observed in aged commercial 6061 Al alloys, where spherical (or needle-shaped) (GP) zones (~5 nm), needle-shaped β″, rod-shaped β′, and disc-shaped β particles have been reported. This result raises the possibility that precipitation behavior may be modified in the presence of a heavily deformed microstructure. According to Kim and Wang (2007), in high-dislocation density regions atomic diffusion is expected to be enhanced by pipe diffusion along the cores of dislocations dispersed at random in the matrix. So, the formation of large spherical particles in the ARBed specimens after the ageing treatment might be associated with increased diffusion from the high dislocation density generated during the ARB process.

3.3. Tensile properties

The ultimate tensile strength (UTS) and elongation variations versus the number of cycles for different heat treatment conditions are shown in Fig. 8(a) and (b), respectively.

From Fig. 8, it can be seen that increasing the number of cycles improved UTS values but decreased elongation values in all the specimens. Also, the increment in UTS and the decrease in elongation are rather small, except in the case of the one-pass samples. Saito et al. (1998) and Tsuji et al. (2002) have stated that UTS and elongation variations in severely deformed materials are governed by the two main strengthening mechanisms: (1) strain hardening, and (2) grain refinement. In the early stages of the ARB process, strain hardening or dislocation strengthening play the main role in enhancing strength and in decreasing elongation, while the formation of submicron subgrains or dislocation cells also contributes to enhanced strength as pointed out by Hansen et al. (2004). At higher cycles, however, higher strength and lower elongation are achieved by grain refinement as the ARB cycles increase. As the effect of work hardening diminishes, gradual evolution of ultra-fine grains will play the main role in improving strength and decreasing elongation. This effect is related to the increasing number of ultra-fine grains and to the largely misoriented grain boundaries.

Fig. 8(a) shows the increasing UTS values after ageing at both temperatures and for any number of cycles. Also, Fig. 8(b) shows that elongation values in all the ARBed specimens increase by ageing treatment. This behavior can be explained by the competition between recovery and precipitation during the ageing process. Due to the recovery during the ageing treatment, dislocation density decreases. However, precipitation also occurs during ageing, which contributes to the enhancement of UTS and strain hardening. It is obvious that the contribution to strength by precipitation is higher than the loss of strength due to recovery and that the overall effect is a simultaneous increase in both UTS and elongation values.

Furthermore, in contrast to UTS results for the ARBed specimen without ageing treatment, the increased values of UTS after ageing at 373 K for 48 h are higher compared to those with ageing at 433 K for 5 h. As mentioned before, the softening effects at 373 K are less than those at 433 K. Also from Fig. 8(a), it is clear that the improved values of UTS for both ageing temperatures with increasing number of cycles are lower compared to those of the ARBed specimen. The decrease is, however, less for 373 K than it is for 433 K. These results can be accounted for by considering the driving force due to the stored deformation energy. By increasing the number of cycles, the driving force for recovery and structure coarsening increases, thereby decreasing the improved UTS values. All the results obtained are in agreement with those obtained for microhardness.

3.4. Fractography

A scanning electron microscopic (SEM) study was undertaken in order to clarify the failure mechanisms in the annealed, ARBed, and ARBed + aged specimens. Fig. 9 illustrates the fracture surfaces after tensile tests of the annealed and ARBed specimens at the first, third, and fifth cycles. Also, the fracture surfaces after the tensile tests of the specimens ARBed + aged at 373 K for 48 h and those ARBed + aged at 433 K for 5 h after 5 cycles are shown in Fig. 10. They reveal that the annealed sample exhibits a typical ductile fracture showing deep equiaxed dimples (Fig. 9(a)). Ductile tensile fractures in most materials have a gray fibrous appearance with equiaxed or hemispheroidal dimples which occur as a result of microvoid formation and coalescence as demonstrated by Gabriel (1998). The shape of the dimples can determine the type of loading that the component experienced during fracture, and the orientation of the dimples reveal the direction of crack extension. Clearly, after ARB process, the samples also show a ductile fracture having dimples but these dimples were not as deep as those in initial material. Fig. 9(b)–(d) (after 1, 3 and 5 ARB cycles) shows that by increasing the number of cycles in the ARBed specimens, the equiaxed dimples become finer in size and shallower. As mentioned before,

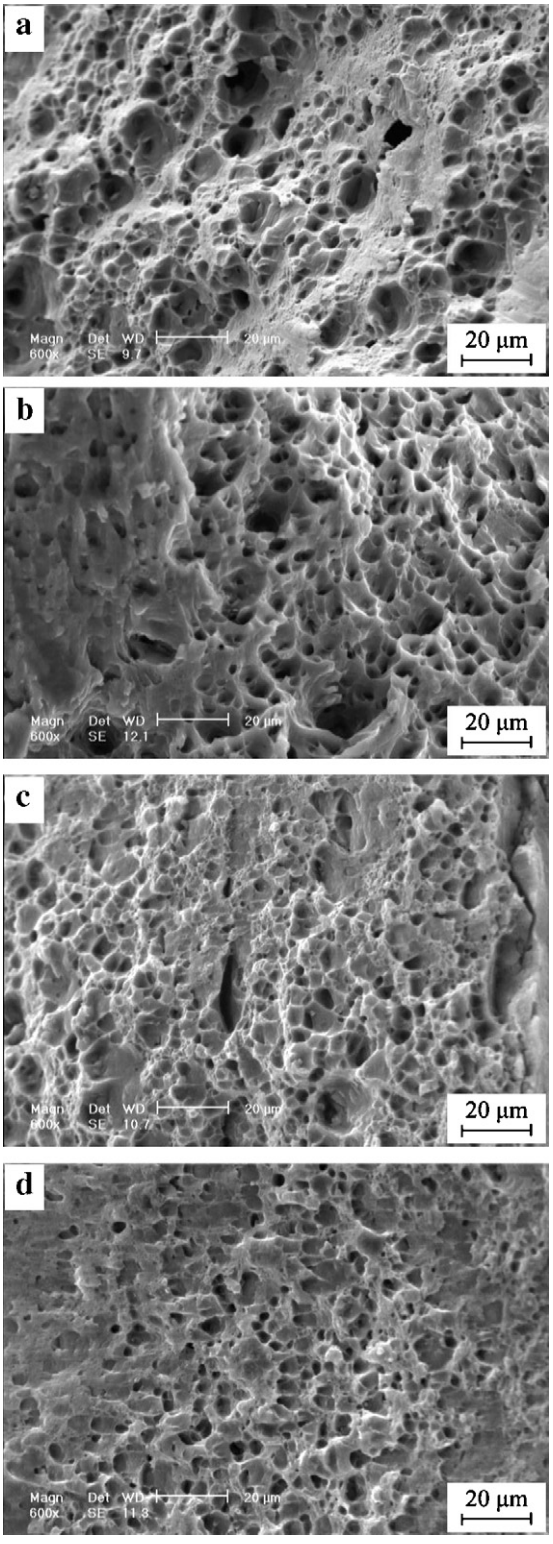

Fig. 9. Fracture surfaces after the tensile test for (a) annealed, (b) 1-cycle ARBed, (c) 3-cycle ARBed, and (d) 5-cycle ARBed samples.

increasing the number of cycles decreased elongation values in ARBed specimens. So, by increasing the number of cycles the plastic deformation until fracture decreased and the size and deepness of dimples reduced.

Based on Fig. 10(a) and (b), the equiaxed dimples become deeper with increasing the ageing temperature as a result of improved ductility. The presence of different particles is visible inside the

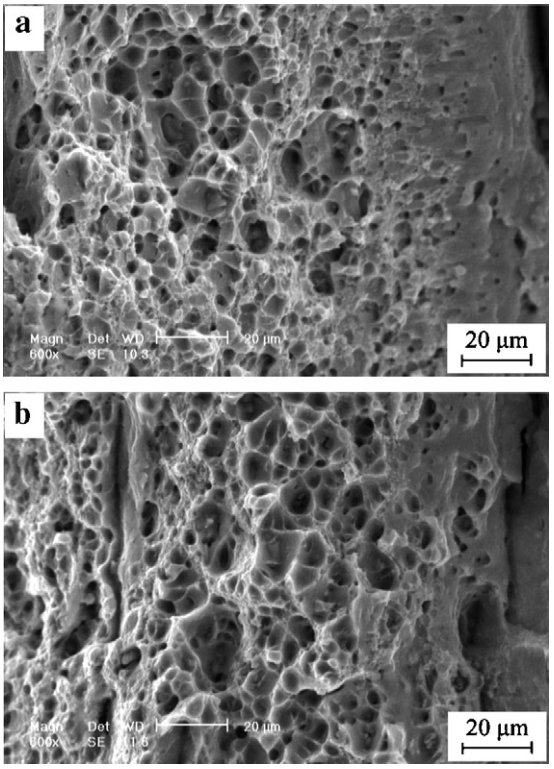

Fig. 10. Fracture surfaces after the tensile test in the 5-cycle ARBed + aged sample at (a) 373 K for 48 h, and (b) 433 K for 5 h.

dimples. It can be seen that these particles provide the sites for the heterogenic nucleation of dimples. Sharma et al. (2009) have stated that, the fracture of tensile specimens was predominantly caused by microvoid coalescence at coarse constituent particles.

4. Conclusion

The ARB process and ageing treatment were used as a technique in this paper to provide an effective alternative for the manufacture of high-strength 6061 aluminum alloy. The mechanical properties of the samples were investigated and related to the microstructure of the material. The conclusions drawn from the results can be summarized as follows:

1. The microhardness and strength values of the ARBed samples increase by increasing the number of ARB cycles and reached up to 113 $HV_{0.1}$ and 362.5 MPa respectively, after five cycles of ARB.
2. Peak-ageing conditions are reached after 5 h of ageing at 433 K and after 48 h of ageing at 373 K for ARBed samples.
3. TEM observations revealed that softening effects in ARBed samples were greater after ageing at 433 K for 5 h than those after ageing at 373 K for 48 h.
4. Strength and elongation improved simultaneously after ageing under both conditions (at 433 K for 5 h and at 373 K for 48 h) in ARBed samples.
5. SEM observation of fracture surfaces showed that the fracture took place by microvoid coalescence at constituent particles in aged specimens.

References

Abis, S., Boeuf, A., Caciuffo, R., Fiorini, P., Magnani, M., Melone, S., 1985. Investigation of Mg_2Si precipitation in an Al–Mg–Si alloy by small angle neutron scattering. J. Nucl. Mater. 135, 181–189.